



Microstructures and mechanical properties of friction hydro-pillar processing overlap welding in API 5L X65 pipeline steel

Y. C. Xu^{1,2} · H. Y. Jing^{1,2} · Q. S. Jia^{1,2} · Y. D. Han^{1,2} · L. Y. Xu^{1,2}

Received: 1 September 2016 / Accepted: 3 January 2018 / Published online: 15 January 2018
© International Institute of Welding 2018

Abstract

This paper exhibits a novel in situ remediation technique named friction hydro-pillar process overlap welding (FHPPOW) to repair the through crack of the structures and components in the harsh environments. In the present work, the effects of welding parameters on the microstructures and mechanical properties of the welding joints are investigated. The defect-free joints can be obtained in a large process window with the rotational speed of 6000–7000 rpm and welding force of 20–40 kN. In the heat-affected zone (HAZ), the interface between the substrate and lap plate can be clearly distinguished. The microstructure of the weld is mainly consisted of the upper bainite. The hardness value in the welding zone is highest and is the lowest in the base material. The pull-out tests of all welds are failure in the stud. Results indicate that the good welding quality can be obtained in these welding conditions. The best results of the cruciform uniaxial tensile and the shear tests are 662.8 and 552 MPa, respectively. The favorable Charpy impact absorbed energy is 68.75 J at 0 °C. The fracture characteristic of Charpy impact tests is brittle fracture with a large area of cleavage.

Keywords FHPPOW · API 5L X65 steel · Microstructures · Mechanical properties

1 Introduction

Defects frequently develop on the engineering structures and industrial components to shorten service life. Repair and maintenance activities become the focus of issue. As far as repair methods are concerned, traditional fusion welding process has been employed in the overwhelming majority of cases. However, fusion welding has caused some problems which include grain growth, hydrogen embrittlement, and slag trapping [1]. Moreover, the severe conditions also limit the usefulness of this process [2–4].

Conventional fusion welding methods have disadvantages inherent to their process, which has encouraged the search for new techniques to obtain a sound welding joint. As a solid-

state joining process, friction hydro-pillar processing (FHPP) derived from friction welding has been developed to replace the fusion welding as a new repair technique. The main features of FHPP are illustrated in Fig. 1. As shown, this novel technique involves a rotating consumable stud rubs against an essentially circular hole under an applied downward force. In general, it accepts arbitrary design geometries of the stud according to needs. The cylindrical and tapered shapes are the most common types. When the stud shape selects taper, this technique can be also termed as friction taper stud welding (FTSW) which belongs to FHPP process. With the stud tip continuous friction against the hole bottom, the sliding surfaces interact to generate a localized plasticized layer filling the gap between the hole and the stud. When the gap is filled completely, the forging force replaced the welding force is applied until the process is finished [5].

Since FHPP was developed by TWI [6, 7] as a new repair method, a lot of researches have been conducted to study this proposed technique. In 1993, Thomas and Nicholas [8] presented additional advantages of the FHPP by focusing on its application in the industry for joining and repairing thick steel components. The researchers stated that as in all friction welding processes, the weld material needed for FHPP is relatively small and the process is easily automated for mass production. Nicholas [9] reported

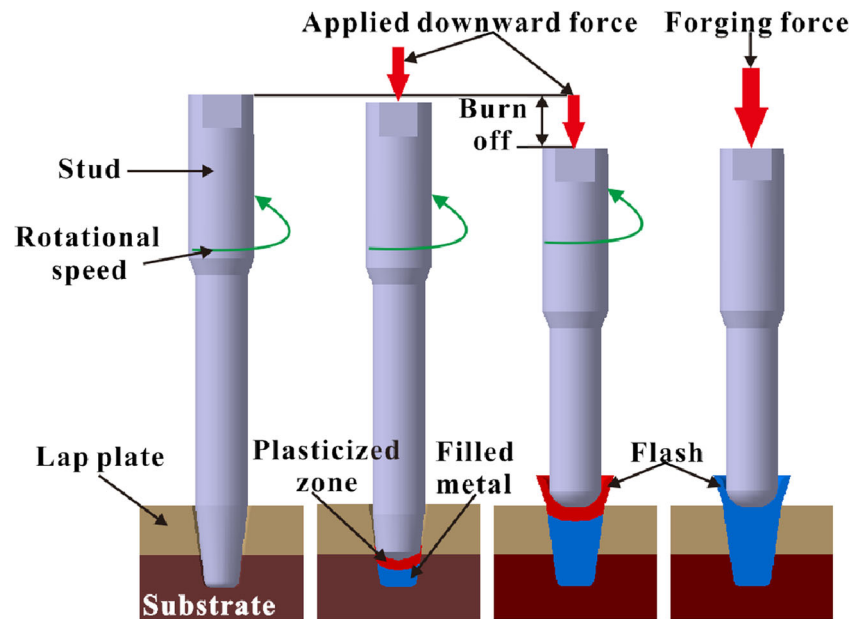
Recommended for publication by Commission IX - Behaviour of Metals Subjected to Welding

✉ L. Y. Xu
xulianyong@tju.edu.cn

¹ School of Materials Science and Engineering, Tianjin University, Tianjin 300072, China

² Tianjin Key Laboratory of Advanced Joining Technology, Tianjin 300072, China

Fig. 1 Schematic illustration of FHPP



the potential advantages of FHPP and was the first to present the microstructure and mechanical properties. This comprehensive report covered the parallel hole configuration as well as the taper hole arrangement. The author found that materials that do not exhibit adequate plastic flow characteristics often responded much better to a tapered joint design. Meyer [5] investigated the bonding mechanism and properties of FHPP in more detail. The stud and hole geometries influenced the bonding quality. The shape of the frictional surface defined the stress distribution and temperature development during the welding process. Moreover, the relationship between the welding parameters and the mechanical properties of welds was also studied. Recently, Chludzinski and his co-workers [10] studied the fracture toughness of FHPP in C-Mn steel using the tapered stud-and-hole configuration. In their work, the fracture toughness of the weld was compared with that of base metal. Moreover, the relationship between fracture toughness values and axial force applied during the entire welding process was studied. Hattings [11] and his co-workers also used tapered experimental samples to present a relationship between force applied during FHPP and mechanical and metallurgical properties of the weld. They indicated that the welding

parameters with high rotational speed and low applied downward force could produce the highest tensile strength of the joint. With increasing of the welding force, the tensile strength value of the weld decreased. There were two major types of the defects in the joint. The most influential defect was the flash crack which could dramatically reduce the tensile strength of the joint.

In order to prevent the components being welded through under the great welding pressure, the working depth of FHPP is usually less than half the thickness of the structures. In other words, this novel technique is generally employed to repair the embedding crack which is located above the half of the damaged structure thickness. However, in the most actual projects, the various through cracks abound in engineering and are easy to detect by professional equipments, especially in pressure vessel and the pipeline. Comparing with the embedding crack, the through crack is much more dangerous and imperative to repair; otherwise, the deficient equipment completely maintain in the operation moratorium state. To deal with this problem, the overlap welding method of FHPP has been proposed as shown in Fig. 2. The through crack is covered with a lap plate and welded all around using FHPP process to fix the lap plate on the broken

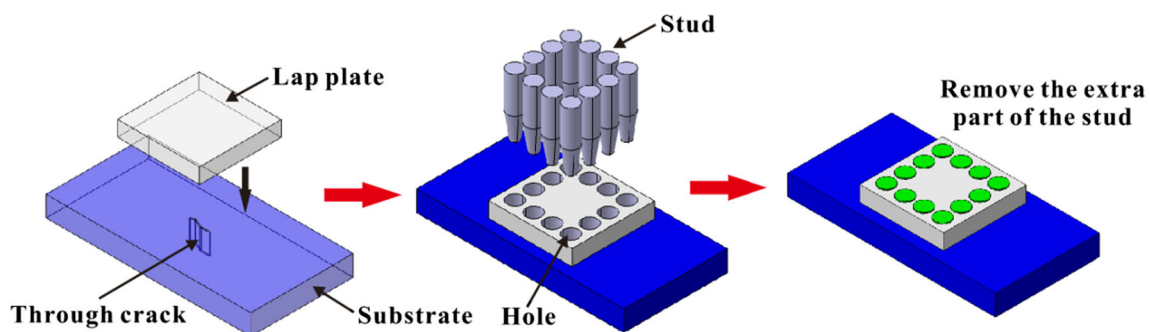


Fig. 2 Schematic illustration of FHPP for repairing through crack

component. The FHPP overlap welding (FHPPOW) process not only inherits the merits of the friction welding but also can solve the problem of the through crack.

In this study, the API 5L X65 pipeline steel is selected as stud and base materials to evaluate the weldability for FHPPOW. The influences on weld quality of the process parameters such as rotational speed and applied downward force are considered. All welds are performed by using self-developed high-performance welding equipment. The characteristic, macrostructure, microstructure, and hardness of the welds are methodically studied. To evaluate the quality of the welds, a pull-out test, a cruciform uniaxial tensile test, a shear test, and a Charpy impact test are conducted. The results are also systematically discussed.

2 Experimental procedure

A 15-mm-thick lap plate and a 20-mm-thick substrate were used in this investigation. The lap plate was closely

connected with substrate through four bolts at each corner. The stud had a 18° taper, and the corresponding hole had a 20° taper. Both stud tip and hole bottom were designed 2 mm rounded corner. Figure 3a gives geometrical details of the specimen. The API 5L X65 pipeline steel according to API 5L standard was selected as the base material for both consumable tool and substrate to carry out the FHPPOW experiment, which the chemical composition was presented in Table 1. The basic mechanical properties of this material are illustrated in Table 2.

All welds were performed using a hydraulically-powered machine. This entire welding system primarily consisted of four major components: a hydraulic unit; a welding head, including a hydraulic fixed motor and a cylinder; valve blocks; and a control system. The maximum power of hydraulic unit is 90 kW, and the maximum axial force is 60 kN. The maximum rotary speed of the hydraulic fixed motor is 8000 rpm, and the maximum torque is 120 Nm. In this study, the rotational speed was selected 6000 and 7000 rpm, while the applied downward

Fig. 3 **a** Geometrical details of the experimental samples. **b** Schematic of the pull-out specimens. **c** Schematic of the cruciform uniaxial tensile specimens. **d** Schematic of the shear specimens. **e** Schematic of the Charpy impact specimens

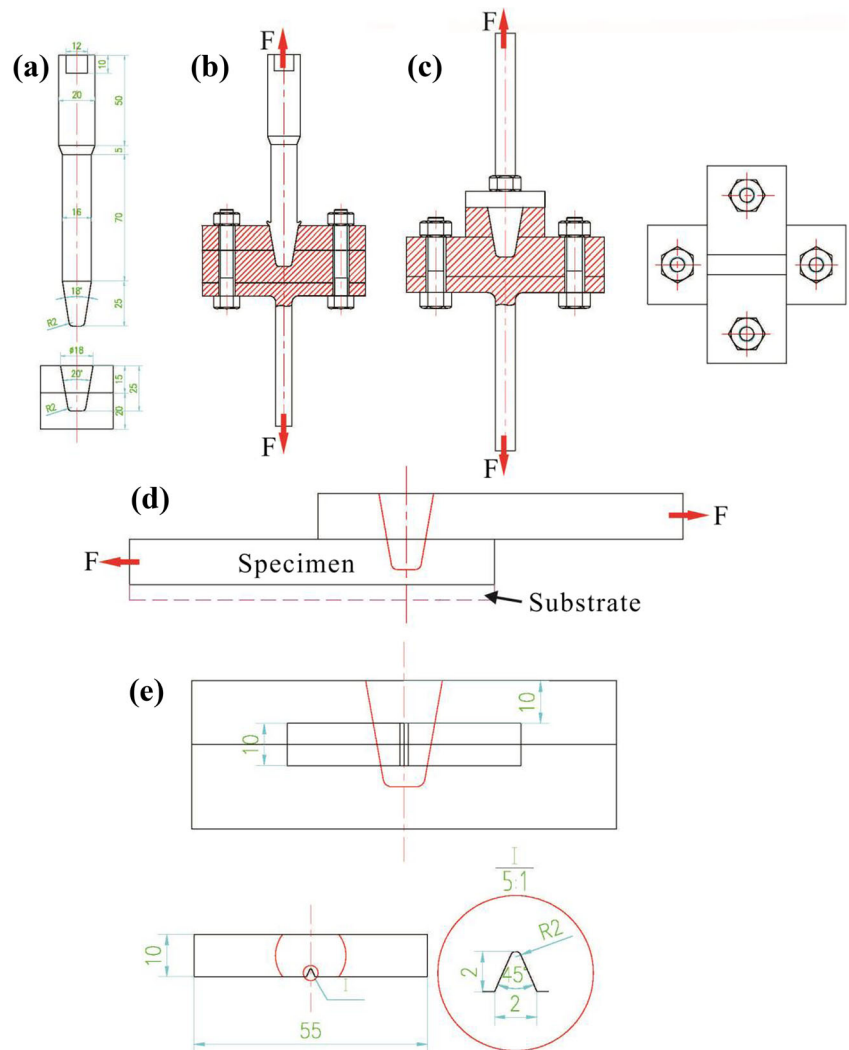


Table 1 Standard chemical composition of API 5L X65 pipeline steel (all values in wt%)

Chemical composition	C	Si	Mn	P	S	Ni	Cr	Nb	Ti	Fe
Standard values	0.059	0.26	1.52	0.01	0.0013	0.455				Balance
Measured values	0.044	0.26	1.5	0.005	0.0006	0.452				Balance

force was changed from 20, 30, and 40 kN as shown in Table 3. During the welding, an additional measurement system was used for acquisition and recording the processing parameters including rotational speed, welding force, and axial displacement of the stud and torque to analyze the characteristics of the welding process.

Once the welds were finished, they were sectioned through the center of the weld zone and mechanically ground. To characterize the macrostructure of the welding specimens, the samples were etched by using 3% HNO₃ + C₂H₅OH solution. Key features of the weld were characterized by using an Olympus SZX16 optical microscope. The micro-structural observation of the weld was conducted by Olympus GX51 optical microscope. A 432SVD Vickers hardness tester was used to evaluate the HV₁₀ hardness distribution of the joints. The measurements were taken in three rows and the spacing of test points was 1 mm, as illustrated in Fig. 5c. As demonstrated in Fig. 3b, c, the pull-out and cruciform uniaxial tensile tests for welds were performed to evaluate the quality of the joints. Moreover, the shear tests of the joints were also conducted as shown in Fig. 3d. The pull-out, cruciform uniaxial tensile, and shear tests were conducted three times in each welding condition on the CCSS-3910 universal electric tension machine with load rate of 5 mm/min. The standard Charpy V-notch samples with dimensions of 10 mm × 10 mm × 55 mm were machined to evaluate the impact toughness of the weld metal at 0 °C using a drop weight impact tester, according to ASTM: E23-02a (standard test method for notched bar impact testing of metallic material). The impact test in each welding condition was also conducted three times. Specimens were extracted machined from all welds at 10 mm distance from the lap plate surface. The notch was oriented normal to the substrate surface at the center of the stud as shown in Fig. 3e. The fracture surfaces of the impact samples were observed using SEM to identify the fracture behavior.

3 Results and discussion

3.1 Process characterization

A measurement system has been designed and built to record and store the welding parameters including rotational speed, axial displacement of the stud, applied downward force, and torque during the welding process. Figure 4 presents the measured welding parameters of sample S1. As indicated in the diagram, four stages including preparation, rubbing, filling, and forging can be divided on the basis of different pressure. In the preparation stage, the stud begins to rotate until reaches the required speed. And then, the piston pushes the rotating stud into the hole. There is no moment of contacting between the stud and the hole. In this stage, the rotation speed holds wave nearby a pre-set value. The applied downward force is almost zero and the torque is stable at 20 Nm. Only the displacement of the stud is increasing at a certain rate. The stud contacted with the bottom of the hole marks the beginning of the rubbing stage. As the stud rubs the bottom of the hole, the torque appears a peak value firstly due to the instantaneous collision. This collision also led to fluctuation of the rotational speed. The applied downward force increases to the specified value over a period of 2 s due to the relaxation of the hydraulic system. With increasing of the friction under the growing applied downward force, the torque is fluctuating sharply. The material of the contacting couple is softened by the frictional heat which is caused by the rubbing. The softened metal on the interface can reduce the torque. Meanwhile, the welding force continuously increases resulting in the growing torque. The displacement increases with the increased burn-off of the stud. The rotation speed is relative constant except for the initial undulation. In the filling stage, a large amount of plasticized metal is generated from the friction surface and pressed out of the interface to fill the gap between the

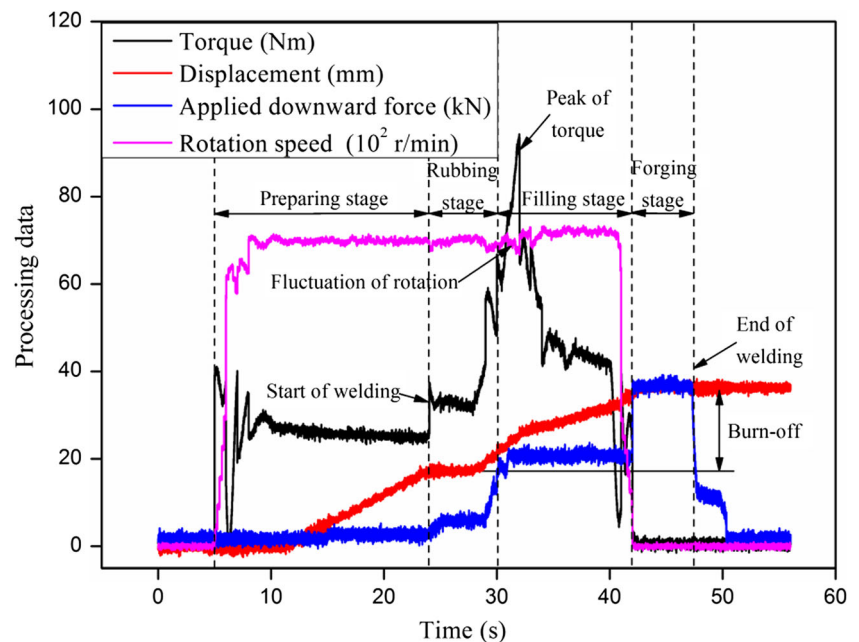
Table 2 Mechanical properties of API 5L X65 pipeline steel

Material	Yield strength (MPa)	Ultimate tensile strength (MPa)	Elongation (%)	Hardness (HV10)	Impact energy at 0 °C (J)
API 5L X65	586.47	716.81	30.3	212.28	≥ 300

Table 3 Full experimental matrix of rotational speed and downward force values

Samples	Welding parameters	
	Rotational speed (rpm)	Applied downward force (kN)
S1	6000	20
S2	6000	30
S3	6000	40
S4	7000	20
S5	7000	30
S6	7000	40

stud and the hole under the constant downward force. The welding force has been reached at the pre-set value and stayed unchanged. As similar with applied downward force, the rotational speed is also stable in this stage except for the initial time of this stage. With the material softening, the torque reduces constantly. The displacement increases at a constant rate due to a constant burn-off rate of the stud. When the pre-set burn-off distance is achieved, a sudden motor stop causes the dramatic change of the torque. The forging stage begins with the spin stopped. A higher forging force is applied at the top of the stud to achieve homogeneous bonding across the whole section. The displacement of the stud remains unchanged. The rotation speed and the torque decrease to zero.

Fig. 4 Acquisition the welding data of S1 during FHPPOW process

3.2 Cross-section features

After etching the welds in a 3% $\text{HNO}_3 + \text{C}_2\text{H}_5\text{OH}$ solution, the weld characteristics and macrostructures are revealed in Fig. 5. All welds are sound with no porosity and without any lack of bonding in all the investigated conditions, especially in the rounded corner where it is very easy to generate flaw due to the high deformation resistance [12]. Observing the cross-section morphologies of the welding specimen, the joints generally consist of an unchanged shape in the lower part of the stud and a region of plastically deformed stud material in the upper part. The several distinct zones including weld zone, inner flash, outer flash, heat-affected zone (HAZ), and base metal can be distinguished as indicated in Fig. 5a. Besides, there are two obvious boundaries in the illustration: one is the interface between the lap plate and substrate, the other is the boundary between the stud and the hole which is defined as bonding line. The plasticized material produced from the stud is pressed to form the weld zone. A part of the plasticized material pressed out of the hole surface under the welding force forms the inner flash. The wall of the hole is squeezed by the transverse pressure to form the outer flash. HAZ is separated from the weld zone through the bonding line. At the beginning of welding process, the friction heat gradually increases from zero resulting in a narrow HAZ. With the rapid generation of the friction heat, the scope of HAZ is expanding. The area of HAZ is deeply affected by welding force but is not influenced by rotational speed. With the increasing of welding force, the area of HAZ is

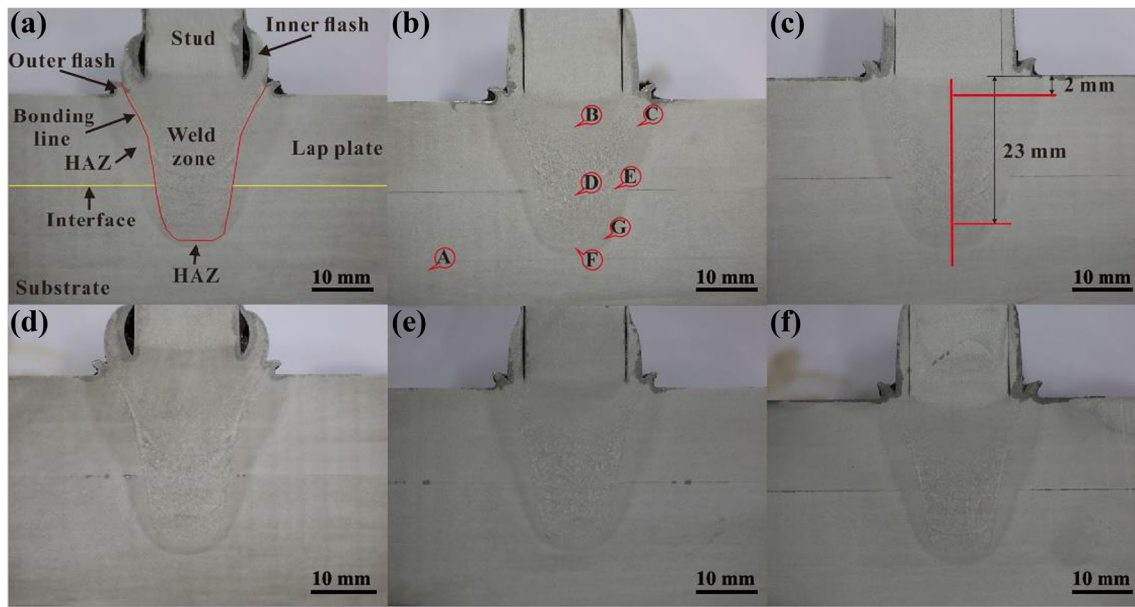


Fig. 5 Macrographs of the samples. **a** S1 and different zones of the joint. **b** S2 and regions for microstructural observations. **c** S3 and hardness testing scheme. **d** S4. **e** S5. **f** S6

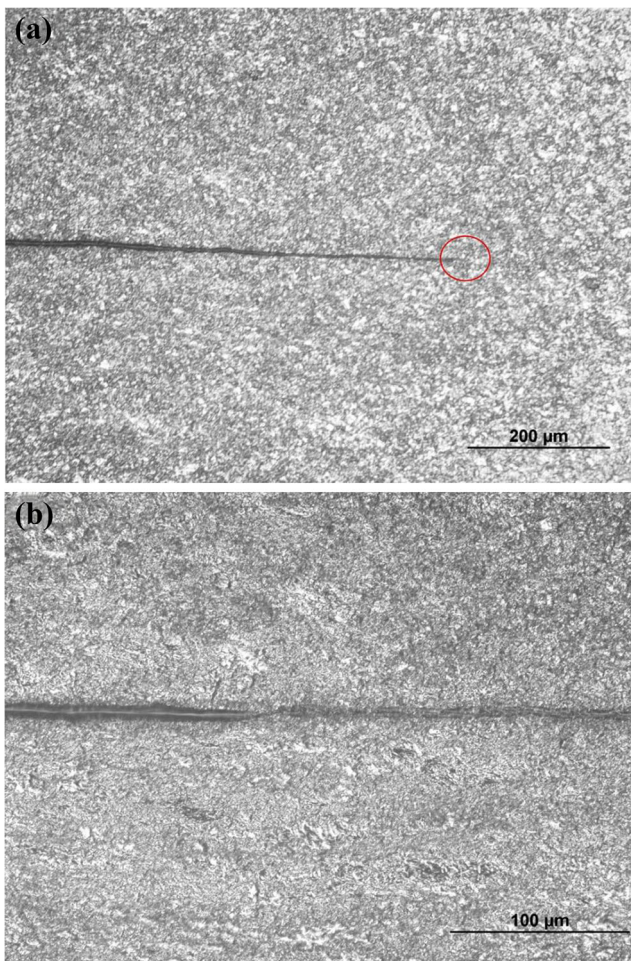


Fig. 6 Microstructures of **a** the interface between substrate and lap plate in HAZ and **b** the filling condition of plasticized material

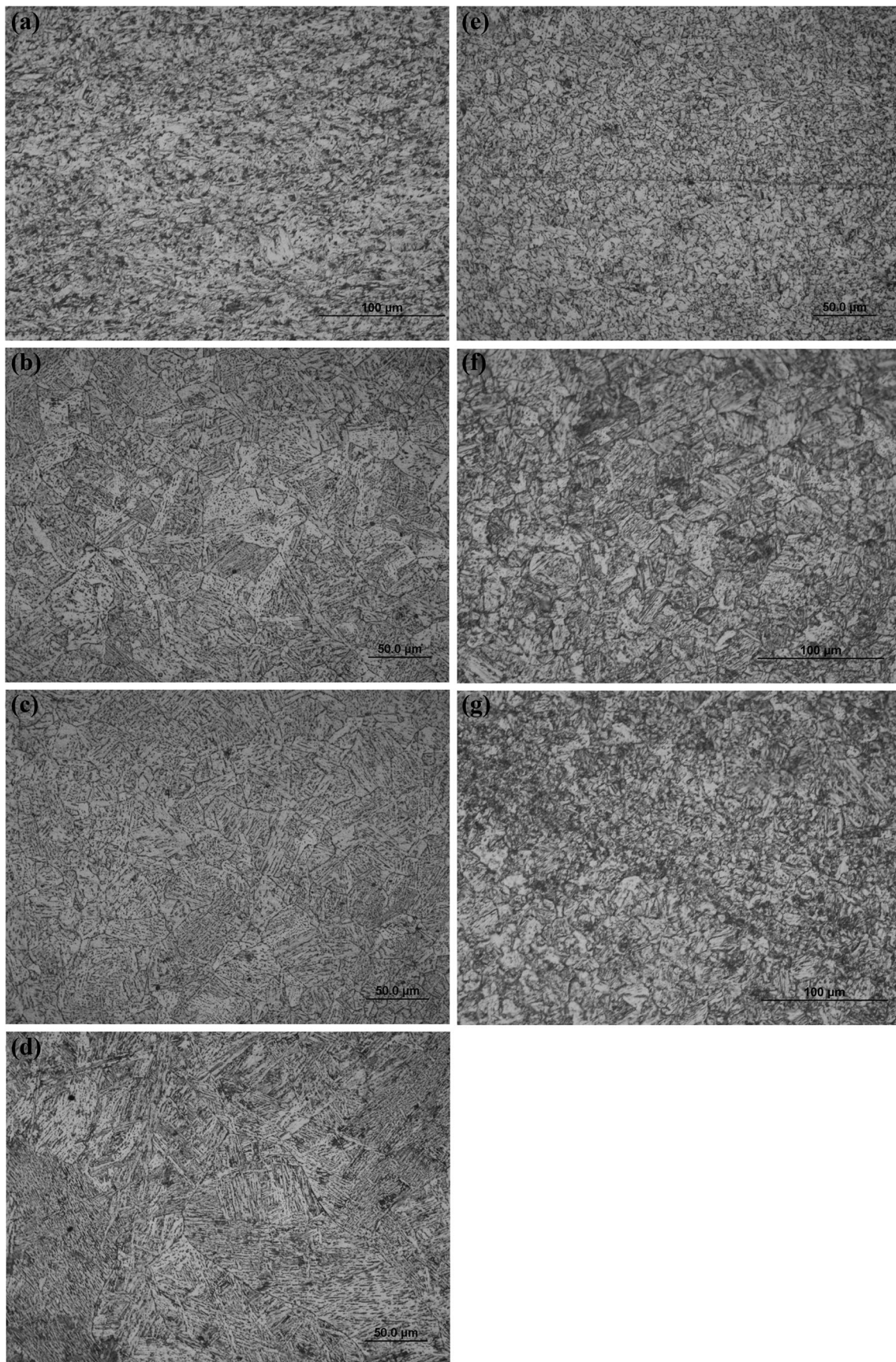
continuous expanding. This is because the high welding force increases the rate of the burn-off, while the welding time is shortened. The heat transfer between the stud and the hole becomes inadequate. Hence, the area of the heated metal correspondingly decreases.

As demonstrated in Fig. 5, the interface between the substrate and the lap plate is hard to distinguish in the HAZ near the welding zone. On the contrary, in the HAZ near the base material, the interface can be clearly differentiated from the macrographs. Figure 6 illustrates the microstructures of the interface in the HAZ. During the welding, the plasticized material is continually extruded into the interface between the substrate and lap plate due to the high temperature and welding force. In Fig. 6b, it can be clearly found that the interface near the welding zone is filled with the plasticized material. The temperature of HAZ area far from the welding zone reduces gradually. The plastic deformation of the material in this area becomes difficult. Hence, the interface of the HAZ far from the welding zone is vacant without any plasticized material.

3.3 Microstructure and hardness

As shown in Fig. 7, the typical microstructure of FHPPOW specimen is observed by optical microscope

Fig. 7 Microstructures. **a** The base material. **b** The upper region of the welding zone. **c** The upper region of the HAZ. **d** The lower region of the welding zone. **e** The middle of the HAZ. **f** The bottom of the HAZ. **g** The corner of the HAZ



and identified according to the ASM Metals Handbook Volume 9-Metallography and Microstructures 2004 [13]. The observing regions are marked A-F in Fig. 5b. As shown in Fig. 7a, the microstructure of the base material

is composed of fine ferrite and pearlite. The microstructure in the weld zone and HAZ is broadly homogenous, which is consisted of upper bainite. As shown in Fig. 7b, the microstructure of the upper region of the weld zone

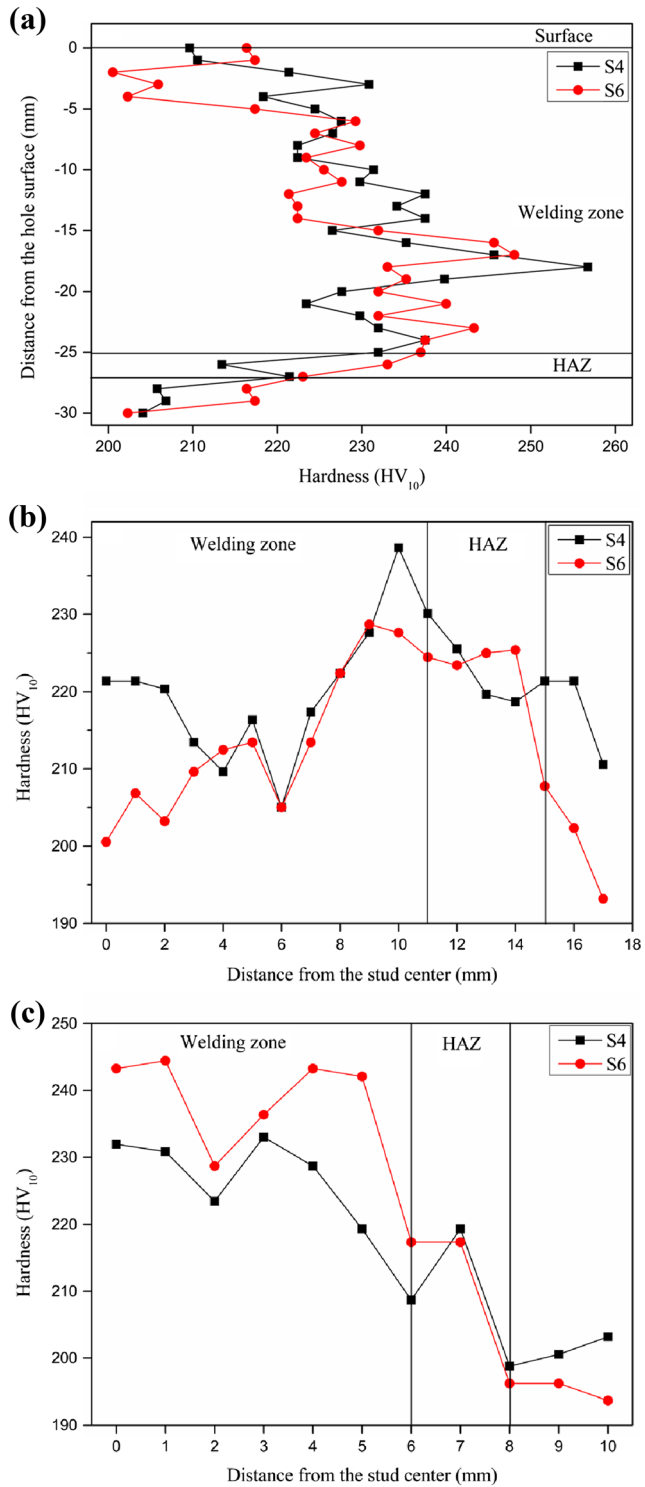


Fig. 8 Hardness distribution of S4 and S6 with the same rotational speed along **a** the middle line, **b** the upper line, and **c** the lower line

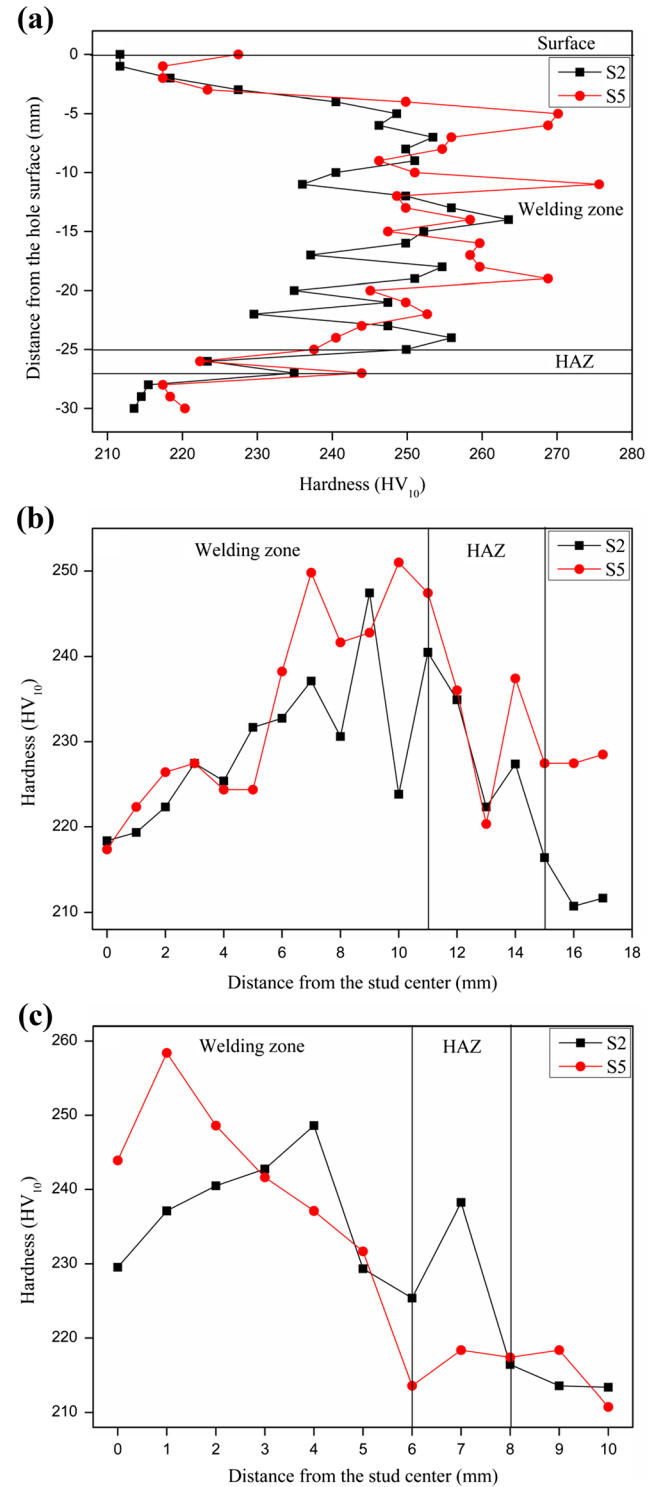
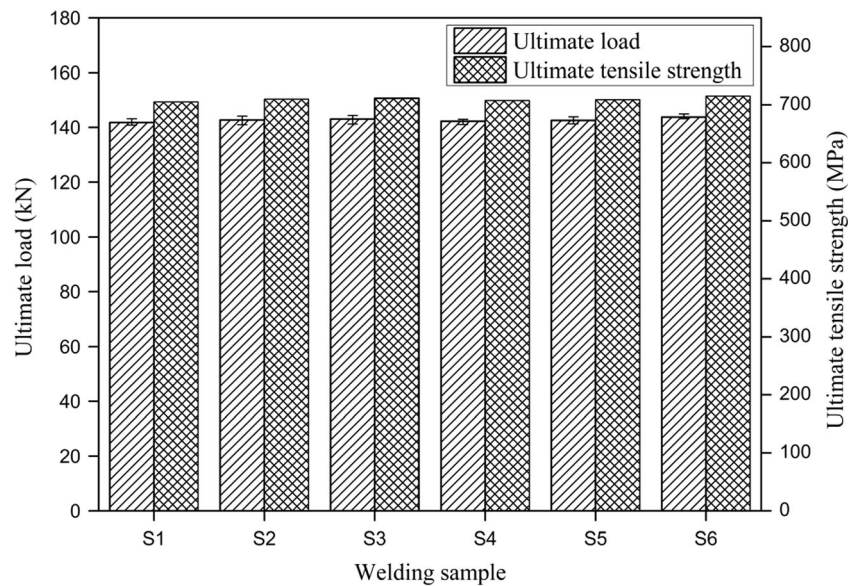


Fig. 9 Hardness distribution of S2 and S5 with the same welding force along **a** the middle line, **b** the upper line, and **c** the lower line

Fig. 10 Pull-out test results of the welds from different welding parameters



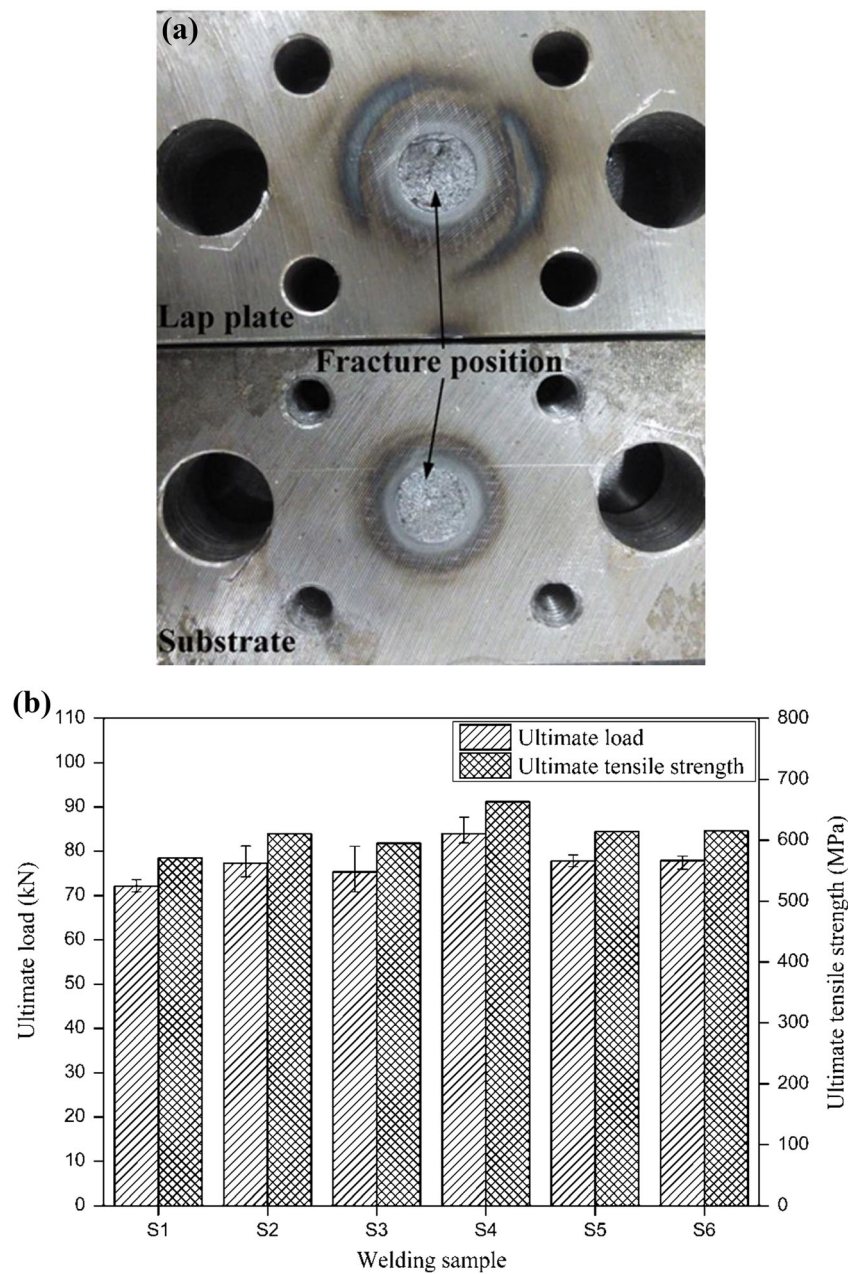
marked B in Fig. 5b contains a large volume of upper bainite. The bunched bainitic ferrite nucleates at the boundary of the prior austenite and grows along the same direction with a high degree of parallelism to one another in the coarse prior austenite grain. The interrupted strip-shaped cementite also has good parallelism which is embedded between the bainitic ferrite laths. The microstructure in the lower weld zone is similar to the upper region of the weld zone as shown in Fig. 7d, but the grain becomes coarse due to the longer heating time and lower cooling rate. The microstructure of Fig. 7c located in upper HAZ marked in Fig. 5c is also consisted of upper bainite. In the middle of HAZ, the microstructure is filled with the upper bainite as shown in Fig. 7e. Compared with Fig. 7d, the grain size in Fig. 7e is much smaller because the severe mechanical agitation results in the grain refining. In the lower HAZ, the microstructure is made up of upper bainite as shown in Fig. 7f. On the hole bottom corner of HAZ, the microstructure is also consisted of upper bainite as shown in Fig. 7g. The grain size in this area is refining due to the mechanical agitation.

To investigate the hardness distribution profile of the joint, the measurements were taken in three rows including center line, 2 mm away from the hole surface, and 2 mm away from the hole bottom as illustrated in Figs. 8 and 9. In Fig. 8a, the black curve presents the hardness survey along the center line of S4 with 7000 rpm and 20 kN. Results exhibit that the highest hardness value appears on the lower area of the welding zone where the most hardness value reaches 256.74 HV₁₀. The micro-structural transformation and strain hardening

make the hardness distribution of the welding zone higher. The microstructure of the welding zone is mainly upper bainite which hardness value is higher than that of the base material. Besides, the severe plastic deformation of the consumable tool caused the strengthening mechanism is throughout the whole welding process. Because of the severe plastic deformation, the hardness value in the welding zone is fluctuant wildly. The hardness near the hole surface is similar to the base material. In this region, the severe plastic deformation is only performed in the forging stage result in inadequately strengthening mechanism. HAZ underneath the hole bottom is also strengthened after welding due to the micro-structural transformation and strain hardening. The hardness survey in this area is higher than that of the base material. As shown in Fig. 8b, c, the hardness distributions in the upper and lower regions of the joint also present the highest value in the welding zone and lowest value in the base material in which the hardness survey shows generally the same behavior as presented in Fig. 8a.

The hardness distribution profiles of S4 and S6 samples with the same rotational speed and different welding force are shown in Fig. 8. The measurements of two welds demonstrate the familiar behavior in the each testing line. With increasing of the welding force, the hardness distribution generally decreases except for the lower region of the welding zone. In Fig. 9, the hardness values of S2 and S5 with the same welding force and different rotational speed is close to each other. Hence, it is believed that the hardness may be influenced by the applied welding force and no significance affected by the rotational speed.

Fig. 11 Fracture appearance (a) and experimental results (b) of the cruciform uniaxial tensile test



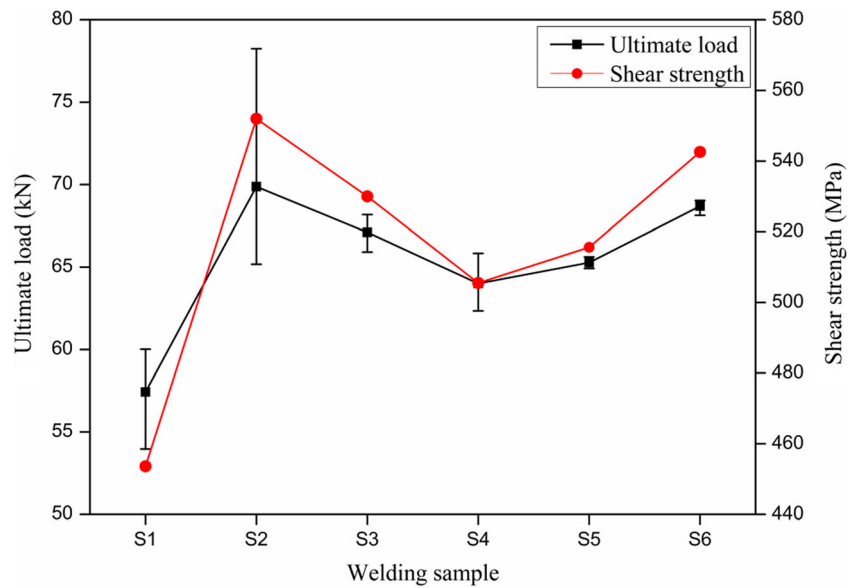
3.4 Pull-out and cruciform uniaxial tensile tests

In order to evaluate the bonding quality of FHPPOW joint, the pull-out test was conducted to reveal the ultimate tensile strength of the welds from all the welding conditions at room temperature. Based on Fig. 10, the experimental results of pull-out test confirm the suitability of the process to perform the favorable tensile strength welds. All joints achieved slightly below the base material strength values with no failure observed within the welded area. Results indicate that the good welding quality can be obtained in these welding

conditions. During the welding, a large amount of friction heat generated by the high-speed spinning consumable tool and the applied downward force spreads around continually. The material of the stud above the lap plate surface is affected by high temperature resulting in decreased mechanical property. Hence, the failure position is on the stud.

According to the specific application of the FHPPOW process, the lap plate suffers the internal pressure via the through crack to separate from the substrate. Accordingly, a novel cruciform uniaxial tensile test has been designed to evaluate the bonding property of the

Fig. 12 Shear properties of the welds with the rotational speed of 6000–7000 rpm and the welding force of 20–40 kN



lap plate and the substrate. The cruciform uniaxial tensile tests show that all the specimens broke at the interface of the lap plate and substrate, as illustrated in Fig. 11a. It can be found that all welds are bonding well at the bottom of the hole and the side wall. The specific morphology of the interface after welding results in the same fracture position. The effective area of the interface is less than that of the stud. Under the same tensile load, the interface of the welding zone suffers the high stress. As shown in Fig. 11b, the best result of 83.96 kN and 662.8 MPa is found at sample S4. The ultimate tensile strength of this joint is lower than that of base material due to the coarse microstructure (in Fig. 7e) caused by the long heating time to reduce the mechanical property of the welding material at the interface.

3.5 Shear strength

Shear strength test results for all welds are illustrated in Fig. 12, which shows that the shear strength of the joint ranges from 453.6 to 552 MPa. All specimens crack and fail at the interface due to the stress concentration. Test S1 with lowest rotational speed (6000 rpm) and welding force (20 kN) gives the worst value of weld shear strength of 453.6 MPa. It can be indicated that the low rotational speed and applied downward force have a negative impact on welding quality. With the increasing of the welding parameters, the shear strength value of the joint also increases rapidly. Compared with the rotational speed, the welding force has a far greater impact on the shear strength of the joint. While S2 and S3 have a lower

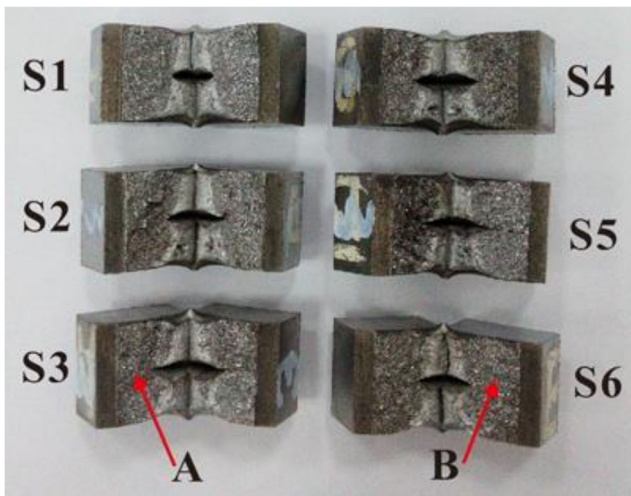


Fig. 13 Fracture surface macrographs of the Charpy impact specimens

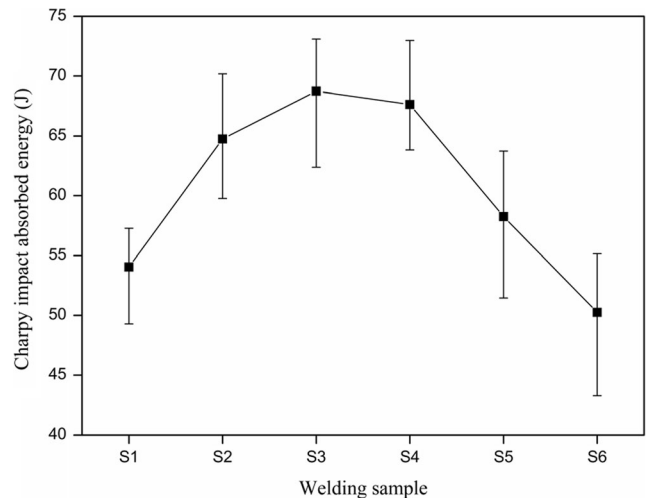
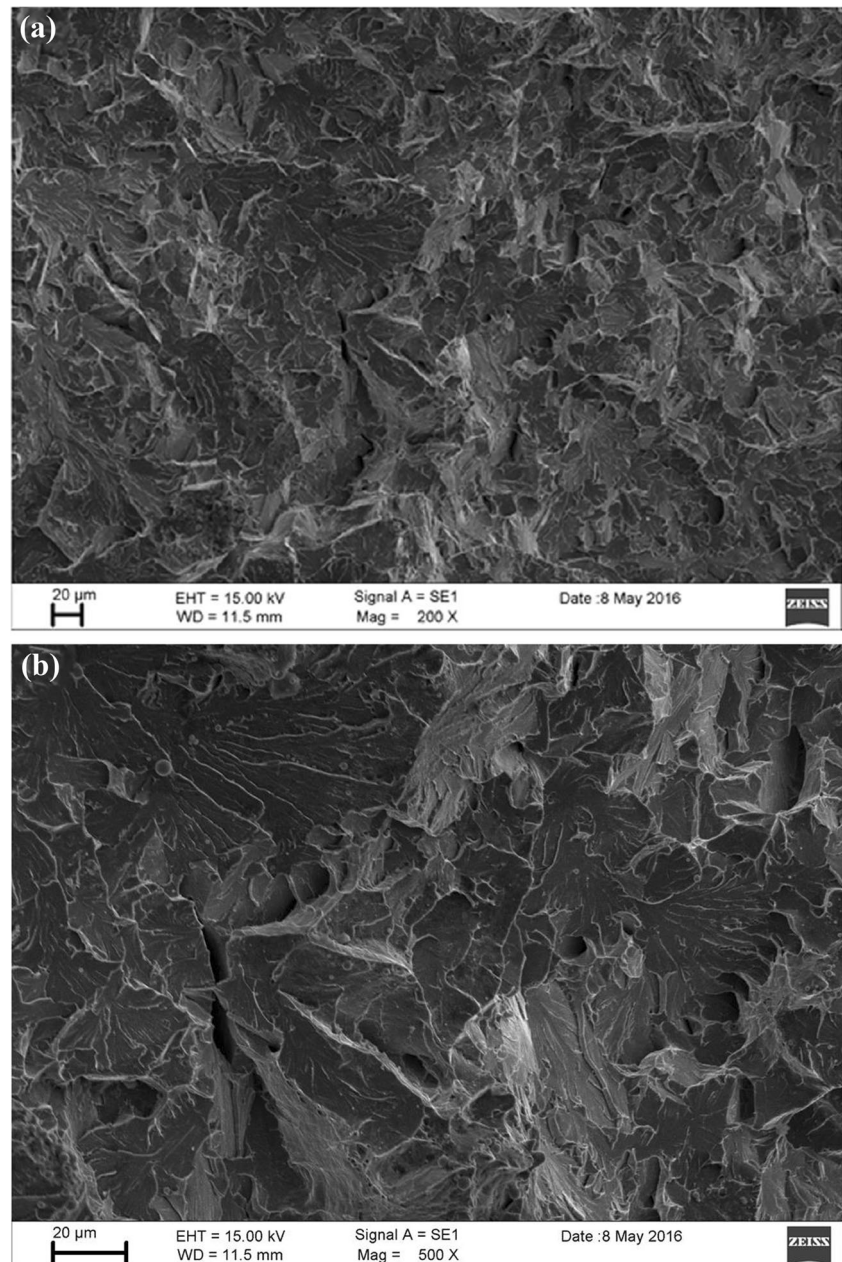


Fig. 14 Charpy impact absorbed energy of the welds at 0 °C

Fig. 15 Fracture morphology in the fracture surface under low (a) and high (b) magnification of S3 that was welded with the rotational speed of 6000 rpm and the welding force of 40 kN



rotational speed, the shear strengths of these two welds are also be enhanced by the higher welding force. Moreover, tests S3 and S6 with the same welding force and different rotational speed show the similar values of the shear strength.

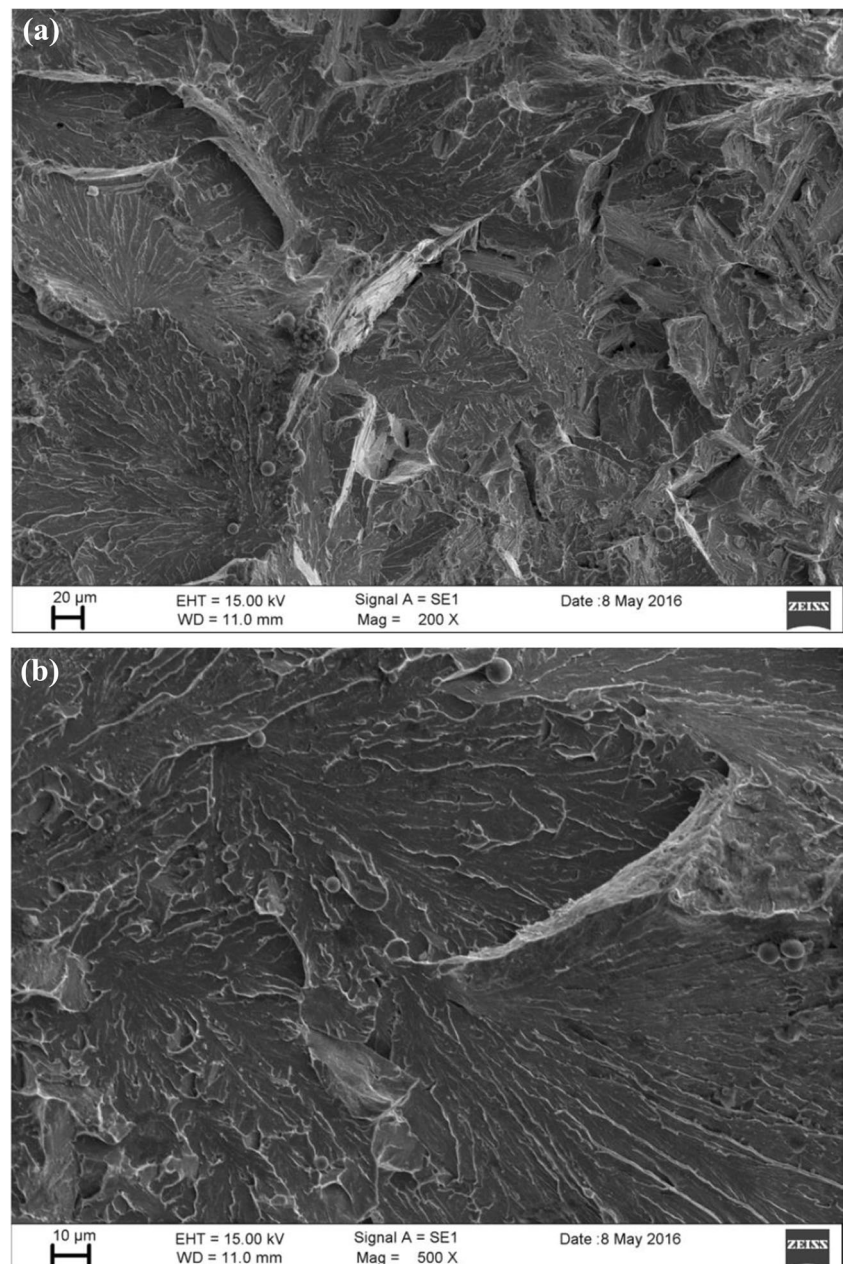
3.6 Charpy impact toughness and fracture morphology

The fracture surface macrographs of all impact samples are shown in Fig. 13. Figure 14 shows the results of the Charpy impact tests which are performed at 0 °C with the notch at the weld zone. For the all impact samples, the best

value was obtained for S3 which has the highest impact energy of 68.75 J with a positive error of 4.34 J and a negative error of 6.37 J. However, the lowest measured value is S6 at the rotational speed of 7000 rpm and the applied downward force of 40 kN. The impact toughness values of the welding zone are lower than that of base material which the Charpy value is higher than 300 J.

The tests S3 and S6 which have the best and worst Charpy impact values are selected to investigate the fracture mechanism. The typical SEM impact fracture morphology in the fracture surface of the specimen S3 with an axial force of 40 kN and a rotational speed of 6000 rpm is shown in Fig. 15. The overall observation of

Fig. 16 Fracture morphology in the fracture surface under low (a) and high (b) magnification of S6 that was welded with the rotational speed of 7000 rpm and the welding force of 40 kN



the fracture surface at the welding zone is consisted of a large volume of cleavage facets with different areas as shown in Fig. 15b. The crack initiation of the cleavage facet forms in the prior austenite grain boundaries and propagates gradually to the grain interior. The crack growth presents the river pattern. It is believed that the fracture mechanism of S3 in the welding zone is brittle characteristic. Figure 16 shows the fracture surface morphology of S6. The fracture surface is dominated by the cleavage plains. The fracture mechanism of S6 is also the brittle fracture.

The obtained impact toughness values of all joints at the welding zone exhibit strongly lower than that of

base material. The microstructure of the welding zone is consisted of the upper bainite which the plastic deformation capacity is poor than that of base material. The welding thermal cycle causes the rapid heating in the welding zone coarsening of the austenite grain and result in the coarse bainite structure.

4 Conclusions

- (1) Friction hydro-pillar process overlap welding (FHPPOW) can be used to repair the through crack for API 5L X65 pipeline steel in the damaged

structures and components. All welds are conducted with the rotational speed of 6000 and 7000 rpm, and the applied downward force of 20–40 kN is defect-free.

- (2) The welding joint is consisted of weld zone, inner flash, outer flash, HAZ, and base metal. The interface between the substrate and lap plate can be distinguished. The plasticized metal is extruded into the interface of the HAZ area near the welding zone. The interface of the HAZ area far from the welding zone is void.
- (3) The microstructure of the joint exhibits the homogeneous features. The joint is dominated by the upper bainite. The hardness value in the welding zone is highest and is the lowest in the base material. The hardness is more influenced by the welding force and no significant affected by the rotational speed.
- (4) The pull-out tests of all welds are failure in the stud. The ultimate strength values are slightly below the base material strength values. The best results of cruciform uniaxial tensile and shear tests are 662.8 and 552 MPa, respectively.
- (5) The best and the worst Charpy impact values are 68.75 and 50.26 J, respectively. The fracture mechanism of all welds is brittle fracture characteristic.

Funding information This research work was financially supported by The National High Technology Research and Development Program (863 Program) of China (Grant No. 2011AA090302).

References

1. N. Christensen, The metallurgy of underwater welding, IIW Conference on Underwater Welding, Tondheim, Norway, Pergamon Press, New York, USA, 71–79
2. Johnson MR (1999) Friction stir welding takes off at Boeing. *Weld J* 78(2):35–39
3. Joelj D (2001) The friction stir welding advantage. *Weld J* 80(5):30–34
4. Mishra RS, Ma ZY (2005) Friction stir welding and processing. *Mater Sci Eng R* 50(1/2):1–78. <https://doi.org/10.1016/j.mser.2005.07.001>
5. Meyer A 2003 Friction hydro pillar processing bonding mechanism and properties, PhD thesis GKSS Forschungszentrum Germany
6. TWI. Leading edge. Friction hydro pillar processing. Connect, June 1992
7. Thomas WM, Temple-Smith P 1997 Friction plug extrusion. UK patent application GB 2306365A
8. Thomas W. and Nicholas D 1993 On trial—a new thick plate joining technique, TWI Connect
9. Nicholas ED 1995 Friction Hydro Pillar Processing, 11th Annual North American Welding Research Conference. 7–9.11.95
10. Chludzinski M, Paes MP, Bastian FL, Strohaecker TR (2012) Fracture toughness of friction hydro-pillar processing welding in C–Mn steel. *Mater Des* 33:340–344. <https://doi.org/10.1016/j.matdes.2011.07.056>
11. Hattingh DG, Bulbring DLH, Els-Botes A, James MN (2011) Process parameter influence on performance of friction taper stud welds in AISI 4140 steel. *Mater Des* 32(6):3421–3430. <https://doi.org/10.1016/j.matdes.2011.02.001>
12. Xu YC, Jing HY, Han YD, Xu LY (2015) Numerical simulation of the effects of various stud and hole configurations on friction hydro-pillar processing. *International J Mechanical Sci* 90:44–52. <https://doi.org/10.1016/j.ijmecsci.2014.10.025>
13. ASM Handbook: Metallography and microstructures. ASM Handbook Committee, Volume 9, 2004